entropy

MDPI

Article

Characterization of the Performance of an XXZ Three-Spin Quantum Battery

Suman Chand [1,*], Dario Ferraro [1,2] and Niccolò Traverso Ziani [1,2]

[1] Dipartimento di Fisica, Università di Genova, Via Dodecaneso 33, 16146 Genova, Italy; dario.ferraro@unige.it (D.F.); niccolo.traverso.ziani@unige.it (N.T.Z.)
[2] CNR-SPIN, Via Dodecaneso 33, 16146 Genova, Italy
* Correspondence: sumanchand.physics@gmail.com

Abstract: Quantum batteries represent a new and promising technological application of quantum mechanics, offering the potential for enhanced energy storage and fast charging. In this work, we study a quantum battery composed of three two-level systems with XXZ coupling operating under open boundary conditions. We investigate the role played by ferromagnetic and antiferromagnetic initial configurations on the charging dynamics of the battery. Two charging mechanisms are explored: static charging, where the battery interacts with a constant classical external field, and harmonic charging, where the field oscillates periodically over time. Our results demonstrate that static charging can be more efficient in the ferromagnetic case, achieving maximum energy due to complete population inversion between the ground and excited states. In contrast, harmonic charging excels in the antiferromagnetic case. By analyzing the stored energy and the average charging power in these two regimes, we highlight the impact of anisotropy on the performance of quantum batteries. Our findings provide valuable insights for optimizing quantum battery performance based on the system's initial state and coupling configuration, paving the way for the study of more efficient quantum devices for energy storage.

Keywords: quantum batteries; xxz spin chain; quantum phase transition

check for updates

Academic Editors: Rosario Lo Franco, Ricardo Puebla and Fernando Gómez-Ruiz

Received: 3 March 2025
Revised: 6 May 2025
Accepted: 8 May 2025
Published: 10 May 2025

Citation: Chand, S.; Ferraro, D.; Traverso Ziani, N. Characterization of the Performance of an XXZ Three-Spin Quantum Battery. *Entropy* **2025**, *27*, 511. https://doi.org/10.3390/e27050511

Copyright: © 2025 by the authors. Licensee MDPI, Basel, Switzerland. This article is an open access article distributed under the terms and conditions of the Creative Commons Attribution (CC BY) license (https://creativecommons.org/licenses/by/4.0/).

1. Introduction

Quantum batteries (QBs) represent a cutting-edge approach to energy storage, leveraging quantum mechanical principles such as coherence and entanglement to achieve superior performance of devices over their classical counterparts [1–4]. The rapid advancement of quantum information science [5,6] and quantum thermodynamics [7–12] has led to an increased interest in exploring the advantages that QBs can offer, particularly in terms of short charging times and improved energy storage capacities [13–37].

Notable models considered for the realization of QBs are spin systems [38–44] where qubits, described as quantum spins, interact under different coupling mechanisms. This allows for the detailed investigation of relevant phenomena such as quantum phase transitions (QPTs) [45–47], which play a significant role in determining the time evolution and the performance of QBs [48] and, more generally, quantum thermal machines [49,50]. Studies have shown that the presence of QPTs can enhance energy storage by reorganizing the ground state of the system, thus impacting the overall charging dynamics [51–54]. This aspect is crucial for understanding how the ground state configuration of a spin system can be harnessed to optimize its performance as a QB [55].

In this direction, our study focuses on exploring a simple model of QB based on three spins in an XXZ configuration, where anisotropy in the interaction leads to distinct

ferromagnetic and antiferromagnetic configurations for the ground state. We investigate the role played by these initial states on the performance of the QB by analyzing the stored energy and average charging power achieved during the charging process. Two distinct charging mechanisms are considered: static charging, where the system is subjected to a constant classical external field, and harmonic charging, where the charging field periodically oscillates over time. Our goal is to study the interplay between the ferromagnetic and antiferromagnetic phases, controlled through the anisotropy parameter Δ, and these two charging protocols to determine the more efficient charging for each initial condition. Throughout this work, we refer to the ground state as ferromagnetic-like or antiferromagnetic-like based on the dominant spin correlations [56,57]. We emphasize that these terms are used descriptively; indeed, in a three-spin system, they do not denote the true thermodynamic phases.

This work aims to provide insights into optimizing QB performance by properly tailoring the charging scheme to the system's initial state. Our results demonstrate that while static charging performs better in the ferromagnetic case, harmonic charging excels in the antiferromagnetic case.

The paper is organized as follows: In Section 2, we describe the QB model, determine the initial conditions, and introduce the different charging mechanisms. In Section 3, we present the results and discuss the QB performance in various configurations. Finally, in Section 4, we provide the conclusions.

2. Model of the QB, Charging Schemes and Figures of Merit

2.1. Anisotropic XXZ Spin QB

We consider a QB consisting of a three-qubit anisotropic XXZ chain under the influence of a uniform external magnetic field h. The system operates under open boundary conditions, as illustrated in Figure 1. The Hamiltonian of the system is described (in units of Planck's constant $\hbar = 1$) as follows:

$$H_B = -J \sum_{n=1}^{2} \left(S_x^{(n)} S_x^{(n+1)} + S_y^{(n)} S_y^{(n+1)} + \Delta S_z^{(n)} S_z^{(n+1)} \right) - 2h \sum_{n=1}^{3} S_z^{(n)}, \tag{1}$$

where S_α^n represents spin operators associated with the n-th site of the chain such that for the considered spin-1/2 system, $S_\alpha^n = \frac{1}{2}\sigma_\alpha^n$ with σ_α^n ($\alpha = x, y, z$) being the conventional Pauli matrices. The magnetic field h acts along the z-axis, J represents the coupling strength between adjacent qubits, and Δ is the anisotropy parameter along the z-axis. For each spin, one can define a ground and an excited state with a spinorial form

$$|g\rangle = \begin{pmatrix} 1 \\ 0 \end{pmatrix}, \quad |e\rangle = \begin{pmatrix} 0 \\ 1 \end{pmatrix}$$

respectively. The eigenstates and eigenvalues of H_B in the three-qubit bare basis $\{|ggg\rangle, |gge\rangle, |geg\rangle, \ldots, |eee\rangle\}$ can be expressed as follows:

$$
\begin{aligned}
|\mathcal{E}_1\rangle &= -|gee\rangle + |eeg\rangle, \qquad \mathcal{E}_1 = h; \\
|\mathcal{E}_2\rangle &= |ggg\rangle, \qquad \mathcal{E}_2 = -3h - \frac{\Delta J}{2}, \\
|\mathcal{E}_3\rangle &= |eee\rangle, \qquad \mathcal{E}_3 = 3h - \frac{\Delta J}{2}, \\
|\mathcal{E}_4\rangle &= -|gge\rangle + |egg\rangle, \qquad \mathcal{E}_4 = -h, \\
|\mathcal{E}_{5,6}\rangle &= |gee\rangle + X_{1,2}|ege\rangle + |eeg\rangle, \qquad \mathcal{E}_{5,6} = \frac{\Delta J}{4} + h \mp 4JY_1, \\
|\mathcal{E}_{7,8}\rangle &= |gge\rangle + X_{3,4}|geg\rangle + |egg\rangle, \qquad \mathcal{E}_{7,8} = \frac{\Delta J}{4} - h \mp 4JY_1,
\end{aligned} \tag{2}
$$

where the parameters $X_{1,2}$, $X_{3,4}$, and Y_1 are defined as follows:

$$
\begin{aligned}
X_{1,2} &= \mp\frac{\sqrt{\Delta^2+8}}{2} + \frac{\Delta}{4} + \frac{4h}{J} \\
X_{3,4} &= \pm\frac{\sqrt{\Delta^2+8}}{2} - \frac{\Delta}{4} \\
Y_1 &= \frac{1}{4}\sqrt{\frac{\Delta^2}{16} + \frac{1}{2}}.
\end{aligned} \tag{3}
$$

Notice that, for the sake of notational convenience, the above states are not normalized.

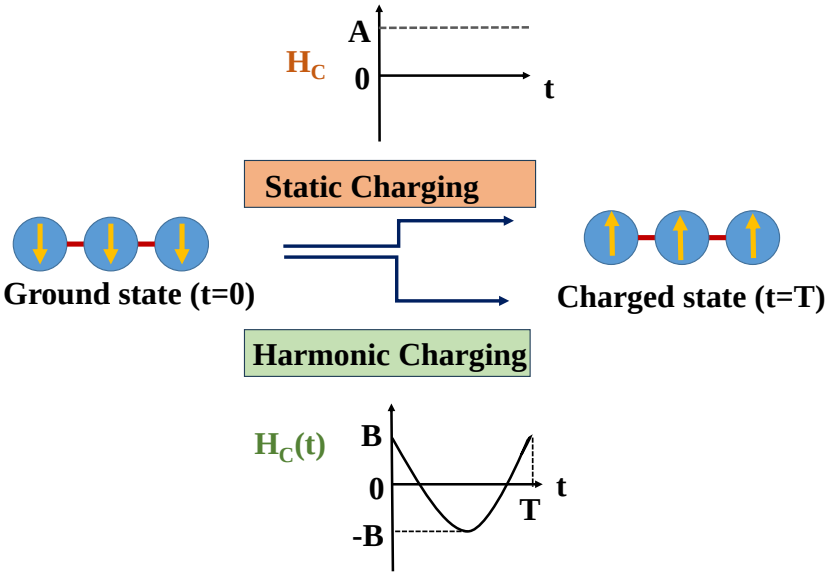


Figure 1. Schematic diagram displaying the charging scheme of the QB. When $t = 0$, the system is in its ground state (ferromagnetic in the example shown). The QB undergoes charging via two schemes: static and harmonic charging. In both cases, the QB interacts with the charging field only for a given time $0 < t < T$, which can be modified to optimize the performance of the device.

Assuming that J is the unit of energy from this point onward, the behavior of the system depends crucially on the anisotropy parameter Δ. Indeed, it is possible to determine a crossover value Δ_C such that for $\Delta > \Delta_C$, the system shows a ferromagnetic ground state, where all spins align along the same direction. Conversely, for $\Delta < \Delta_C$, the ground state of the system exhibits an antiferromagnetic behavior. This transition occurs at $\Delta = \Delta_C$, which separates the ferromagnetic and antiferromagnetic ground states and plays a major role in the energy storage capabilities of the present device, as will be clearer in the following.

Notice that due to the complexity of the calculations involved, these considerations, as well as the precise value of the crossover parameter Δ_C, have been derived from a numerical analysis.

To clarify our terminology, we now explicitly state that Δ_C does not represent a critical value in the sense of a true phase transition but rather a crossover point in our finite three-spin system. In the thermodynamic limit ($N \to \infty$), the XXZ chain exhibits a genuine antiferromagnetic phase. However, in our small system with $N = 3$, Δ_C marks a qualitative shift in ground-state properties. Specifically, we define Δ_C as the value of Δ at which the ground state undergoes an energy level crossing (from $\mathcal{E}_2$ to $\mathcal{E}_7$), transitioning from a ferromagnetic-like configuration, $|\mathcal{E}_2\rangle$ ($\Delta > \Delta_C$), to a state exhibiting antiferromagnetic correlations, $|\mathcal{E}_7\rangle$ ($\Delta < \Delta_C$). This crossover is further supported by the behavior of the nearest-neighbor spin correlation function and the antiferromagnetic structure factor, both of which exhibit a qualitative change around Δ_C. To maintain consistency with the terminology used in larger systems, we retain the designation Δ_C while explicitly clarifying that it signifies a finite-size crossover rather than a true critical point.

2.2. Charging Protocols

In this section, we introduce two distinct charging mechanisms for the QB: static and harmonic charging. For both of them, we will study the time evolution of the QB and evaluate its stored energy and average charging power (see below). At time $t = 0$, the QB is initialized in its ground state whose nature, as stated above, depends on the value of the anisotropy Δ. The system then evolves under the influence of a charging field up to a time $t = T$ carefully chosen to reach a maximally charged state. The time evolution is unitary, and we will approach it in two different ways. We will first assume that the QB Hamiltonian H_B is only used to fix the initial conditions of the system and that the unitary evolution is induced by a, possibly time-dependent, charging Hamiltonian $H_C(t)$ [58]. During this process, the battery Hamiltonian H_B is therefore turned off to focus solely on the charging mechanism's efficiency, inspired by similar approaches in two-level quantum systems like the Rabi model [39,59,60]. Specifically, the charging Hamiltonian H_C is turned on at $t = 0$, driving the system's evolution and injecting energy into the battery. At a chosen time $t = T$, when the stored energy reaches a maximum, the charging Hamiltonian is turned off, and the system subsequently evolves again under the battery Hamiltonian H_B. After, we will consider a more experimentally feasible situation where the unitary evolution is induced by the total Hamiltonian $H_B + H_C(t)$. The precise expressions considered for $H_C(t)$ are discussed in the following, and the problem will be approached by numerically solving the Schödinger equations.

2.2.1. Static Charging

The static charging Hamiltonian is given by the following:

$$H_C = A \sum_{n=1}^{3} S_x^{(n)}, \tag{4}$$

where A is the charging amplitude and $S_x^{(n)}$ are the spin operators along the x direction for the n-th spin of the chain.

2.2.2. Harmonic Charging

In this case, the system is exposed to the periodic time-dependent driving field

$$H_C(t) = B \cos(\omega t) \sum_{n=1}^{3} S_x^{(n)}, \tag{5}$$

where B is the amplitude of the harmonic driving field and ω is the modulation frequency. Also, in this case, we assume that the harmonic charging field is applied up to a time $t = T$ that needs to be chosen in such a way as to optimize the performance of the QB. This optimization will be discussed in the subsequent sections.

We choose the charging Hamiltonians $H_C = A\sum_n S_x^{(n)}$ (static) and $H_C(t) = B\cos(\omega t)\sum_n S_x^{(n)}$ (harmonic) representative forms of uniform driving acting on the spins, commonly used in the quantum battery literature [1,38,61–64]. These operators rotate all spins uniformly and can be implemented using standard transverse fields in trapped-ion or superconducting qubit systems [65,66], while they may not be optimal in a control-theoretic sense, they provide analytically tractable and physically realizable testbeds to assess the influence of anisotropy in the battery Hamiltonian H_B.

2.3. Stored Energy and Averaged Charging Power

The total energy stored in the QB at a given time t, indicated as $E(t)$, is defined as the difference between the energy of the system in the evolved state and the initial state [16]:

$$E(t) = \mathrm{Tr}(H_B\rho(t)) - \mathrm{Tr}(H_B\rho(0)), \tag{6}$$

where $\rho(t)$ is the density matrix of the system at time t, with $\rho(0)$ representing the initial state. This definition captures the energy absorbed from the charging process that is stored in the battery, relative to its ground-state energy. In our charging protocol, we consider two distinct approaches to unitary evolution. In the first, the battery Hamiltonian H_B is used solely to define the initial state, and the system evolves under a charging Hamiltonian $H_C(t)$, which is externally switched on at $t = 0$ and off at a chosen time $t = T$. In the second, more experimentally realistic scenario, the system evolves under the full Hamiltonian $H(t) = H_B + H_C(t)$ throughout the charging process. In both cases, energy is supplied to the system via the externally controlled charger $H_C(t)$. Even in the static case where H_C is time-independent, its sudden activation at $t = 0$ injects energy into the system. In the harmonic case, the time-dependent form of $H_C(t)$ provides continuous periodic energy injection. Although the evolution remains unitary, it is driven by external control, and energy is not conserved with respect to the battery Hamiltonian H_B. The stored energy $E(t)$ quantifies the net energy absorbed by the system, using H_B as the observable to measure useful energy. Since H_B is not necessarily part of the time-evolution operator during charging, $E(t)$ reflects the extractable energy once $H_C(t)$ is turned off. The corresponding average charging power for a given time t is given by the following:

$$P(t) = \frac{E(t)}{t}. \tag{7}$$

The goal of the charging process is to choose the time $t = T$ to maximize the stored energy or the maximum charging power. Notice that, in general, these two times do not coincide; therefore, the choice has to be made taking into account the specific figure of merit relevant to the actual purpose of the considered QB. In particular, the maximum average charging power, defined as the total stored energy divided by the elapsed time, occurs at an intermediate time when the energy storage rate is highest. Stored energy, however, continues to increase beyond this point, reaching its maximum at a later time. This discrepancy arises because average power reflects the average rate of energy storage over time, while stored energy reflects the total accumulated energy. Our results reflect this effect: average power peaks when the charging rate is highest, whereas energy reaches its maximum later as the system approaches saturation.

In this study, we have explored the role of initial conditions and charging protocols. However, optimizing charging time presents an interesting avenue for future research. A systematic analysis should investigate how charging time and power depend on the battery Hamiltonian H_B parameters, ensuring that the ground state remains within the same phase (ferromagnetic or antiferromagnetic). This would help identify parameter regimes that enable faster charging or higher stored energy.

As stated above, the QB is initialized in the ground state of H_B, corresponding to a zero-temperature state. The effect of the initial state on the charging dynamics is highly dependent on the anisotropy parameter Δ, which controls the nature of the ground state. By comparing the performance of the quantum battery under the previously discussed charging schemes, we can analyze the role of the form of the initial state on the performance of the QB. This allows us to identify the optimal charging strategy based on the QB's initial conditions and the specific charging protocol.

3. Charging Performance

In this section, we study the QB charging considering as initial state both the ferromagnetic and antiferromagnetic ground state (characterized by different values of the anisotropy Δ) and under the influence of the static and the harmonic charging field.

3.1. Static Charging with Ferromagnetic and Antiferromagnetic Initial State

We begin by considering the static charging, governed by the charging Hamiltonian $H_C = A\sum_{n=1}^{3} S_x^{(n)}$ (see Equation (4)), where we assume the driving amplitude $A = 1$.

In this case, the charging process is described by the simple time evolution operator $U(t) = \exp(-iH_C t)$, with the QB Hamiltonian H_B turned off during the charging process (see Section 2.2). Numerically, we find that for a coupling strength of $J = 1$ and a magnetic field strength of $h = 1$, the crossover value of the anisotropy parameter is $\Delta_C = -1.58$. According to this, we will study the QB ground state for two values of the anisotropy:

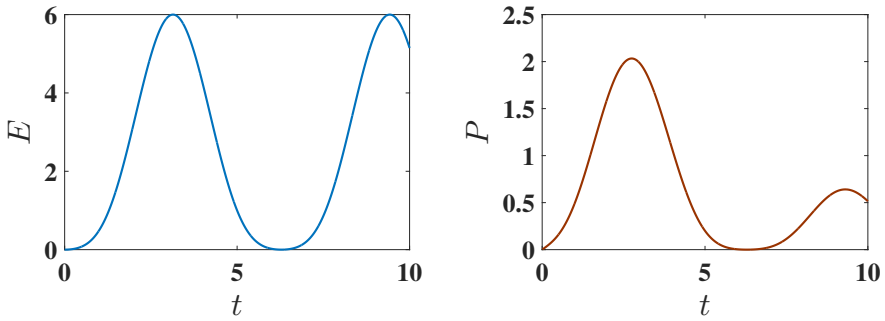
- $\Delta = -1.5 > \Delta_C$: Ferromagnetic ground state.
- $\Delta = -1.6 < \Delta_C$: Antiferromagnetic ground state.

3.1.1. Ferromagnetic Ground State ($\Delta = -1.5$):

Here, all spins are aligned in the same direction. Within the present choice of parameters, the initial energy of the battery in this configuration is $E_{\text{Initial}} = -2.25$, corresponding to the state where all three spins are individually in their ground state. The battery is considered fully charged when all three spins are in their individually excited state, resulting in a final energy $E_{\text{Final}} = 3.75$. Therefore, the maximum energy that can be stored in the QB is as follows:

$$E_{\max} = E_{\text{Final}} - E_{\text{Initial}} = 6.$$

As shown in Figure 2a, this maximum possible energy can indeed be achieved. This is due to the fact that the considered static charging leads to a complete population swap between the ground state ($|\mathcal{E}_2\rangle = |ggg\rangle$) and the excited state ($|\mathcal{E}_3\rangle = |eee\rangle$) of the system, as shown in Figure 3. This efficient population transfer allows the complete charge of the QB by applying a static field.



(a) (b)

Figure 2. Behavior of (**a**) stored energy $E(t)$ and (**b**) average charging power $P(t)$ of the QB as a function of charging time t for $\Delta = -1.5$, corresponding to the ferromagnetic ground state. The charging is performed using the static field $U(t) = \exp(-iH_C t)$. Other parameters used are $J = 1$, $h = 1$, and $A = 1$.

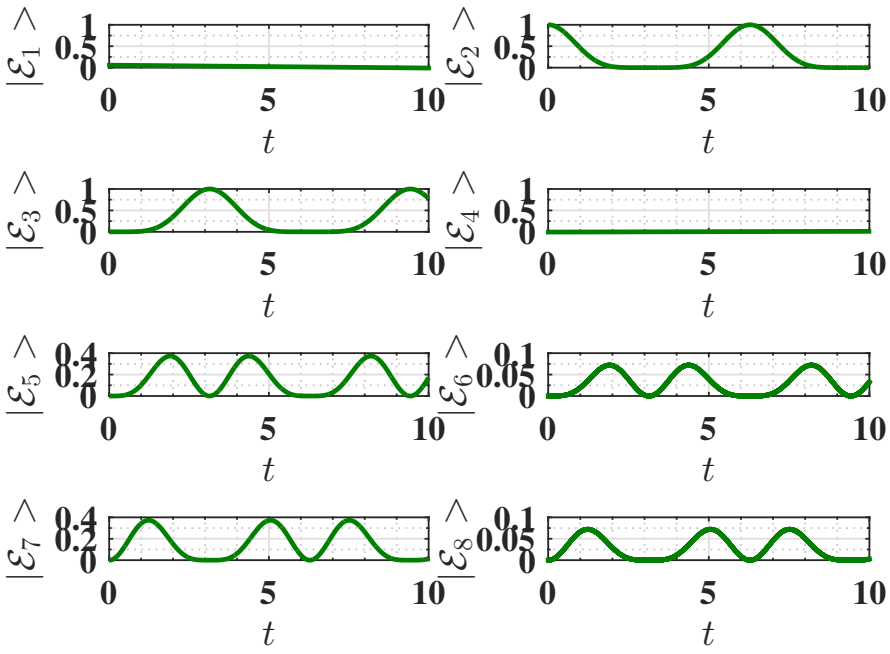


Figure 3. Behavior of the eigenstate populations (see Equation (2)) as a function of charging time t for $\Delta = -1.5$, corresponding to the ferromagnetic ground state. The charging is performed using the static field $U(t) = \exp(-iH_C t)$. The parameters are the same as Figure 2. We recall that in our notation, $|\mathcal{E}_2\rangle$ is the ground state, and $|\mathcal{E}_3\rangle$ is the highest excited state (see Equation (2)).

3.1.2. Antiferromagnetic Ground State ($\Delta = -1.6$):

In this regime, the spins are not individually in their ground states but instead start in a superposition state of the form

$$|\Psi\rangle = C_1|gge\rangle + C_2|geg\rangle + C_3|egg\rangle,$$

where C_1, C_2, and C_3 are constants determined by the values of J and h. For the considered choice of parameters, one has $C_1 = C_3 = 0.3562$, and $C_2 = 0.8638$, satisfying the constraint $C_1^2 + C_2^2 + C_3^2 = 1$ as expected. In this case, the initial energy of the battery is $E_{\text{Initial}} = -2.2124$, and the final energy when fully charged is $E_{\text{Final}} = 3.8000$. Thus, the maximum energy that can be achieved is as follows:

$$E_{\max} = E_{\text{Final}} - E_{\text{Initial}} = 6.0124.$$

Notice that this value crucially depends on the magnitude of the parameter Δ.

As shown in Figure 4a, the QB initialized in the antiferromagnetic ground state can only reach roughly half of this maximum energy due to incomplete population transfer between the ground state $|\mathcal{E}_7\rangle$ and the excited state $|\mathcal{E}_3\rangle$. This incomplete population swap can be seen in Figure 5.

The efficiency of charging depends on the interplay between the battery Hamiltonian H_B and the charging Hamiltonian H_C, while the antiferromagnetic initial state showed poor performances for our chosen H_C, we extend our discussion to different charging schemes based on theoretical considerations. Our findings suggest that an appropriately chosen H_C can significantly enhance charging performance. In particular, a uniform transverse field appears to be the most effective charger across both ferromagnetic and antiferromagnetic states. The staggered field may perform comparably to the transverse field for ferromagnetic states but seems less effective for antiferromagnetic states. Meanwhile, a Heisenberg-type interaction is expected to be inefficient in both cases.

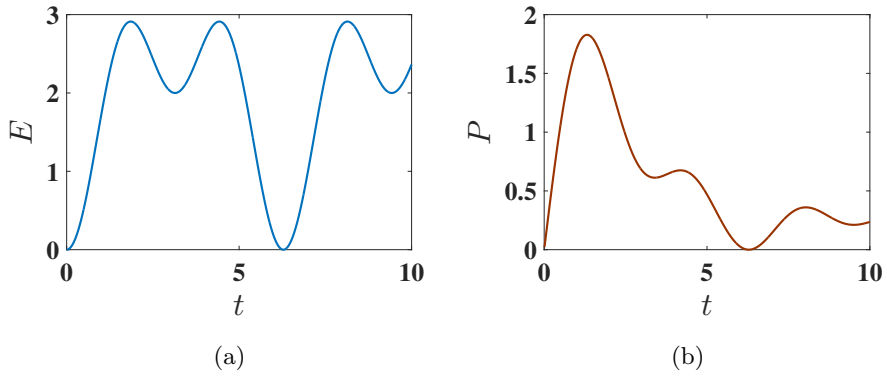


Figure 4. Behavior of (**a**) the stored energy $E(t)$ and (**b**) the average power $P(t)$ of the battery as a function of charging time t for $\Delta = -1.6$, corresponding to the antiferromagnetic ground state. The charging is performed using the static charging field described by $U(t) = \exp(-iH_C t)$. Other parameters are the same as Figure 2.

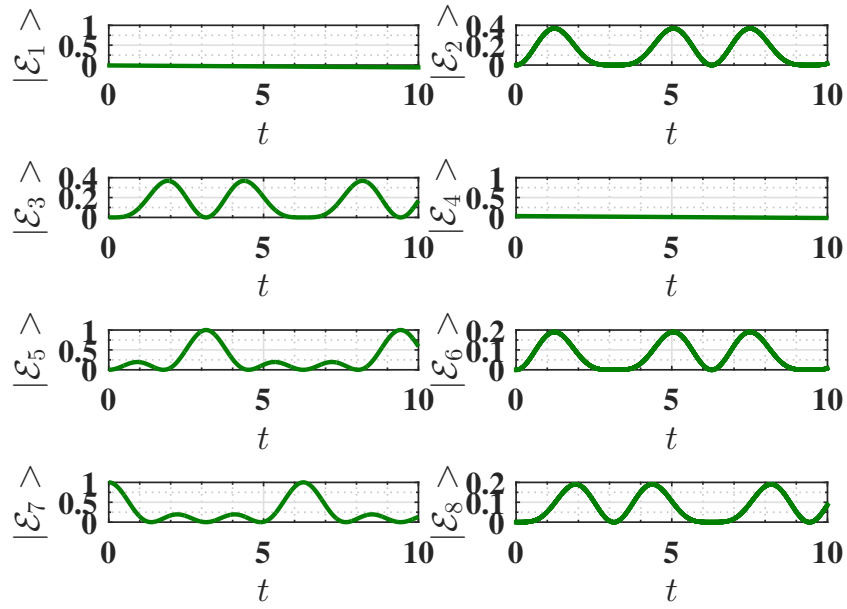


Figure 5. Behavior of the eigenstate populations (see Equation (2)) as a function of charging time t for $\Delta = -1.6$, corresponding to the antiferromagnetic ground state. The charging is performed using the static field $U(t) = \exp(-iH_C t)$. Other parameters are the same as Figure 2. We recall that in our notation, $|\mathcal{E}_7\rangle$ is the ground state, and $|\mathcal{E}_3\rangle$ is the highest excited state (see Equation (2)).

3.1.3. Average Charging Power

Comparing the average charging power $P(t)$ for the ferromagnetic and antiferromagnetic initial conditions, we observe that its maximum $P_{\max}$ is higher for the ferromagnetic ground state (see the comparison between Figures 2b and 4b). However, interestingly, in the antiferromagnetic ground state, the maximum power is reached in a shorter time compared to the ferromagnetic ground state. This indicates that, for this initial condition, one has a faster but less complete population transfer.

3.2. Harmonic Charging with Ferromagnetic and Antiferromagnetic Initial State

In this subsection, we explore the performance of the QB under harmonic charging. The time-dependent Hamiltonian governing the charging process is $H_C(t) = B\cos(\omega t)\sum_{n=1}^{3} S_x^{(n)}$ (see Equation (5)), where we assume the driving amplitude $B = 1$ and the modulation frequency of the harmonic field $\omega = 1$. The time evolution of the QB is then described by the unitary operator $U(t) = \mathcal{T}\exp(-i\int_0^t H_C(t')dt')$, where $\mathcal{T}$ indicates the time-ordering. Here, the QB Hamiltonian H_B only imposes the initial conditions and is turned off during charging (see Section 2.2).

This protocol allows us to analyze how the oscillatory nature of the harmonic field impacts the QB's charging efficiency for both ferromagnetic and antiferromagnetic initial states.

3.2.1. Ferromagnetic Ground State ($\Delta = -1.5$)

As discussed above, here we have $E_{\max} = 6$. However, as shown in Figure 6a, the QB does not reach the maximum energy under harmonic charging due to the incomplete population transfer between the ground state ($|\mathcal{E}_2\rangle = |ggg\rangle$) and the excited state ($|\mathcal{E}_3\rangle = |eee\rangle$), as indicated by the eigenstate population dynamics shown in Figure 7. In this case, the oscillatory nature of the harmonic field disrupts the efficient population swap observed in static charging. Consequently, the QB achieves a lower energy output than the static field case.

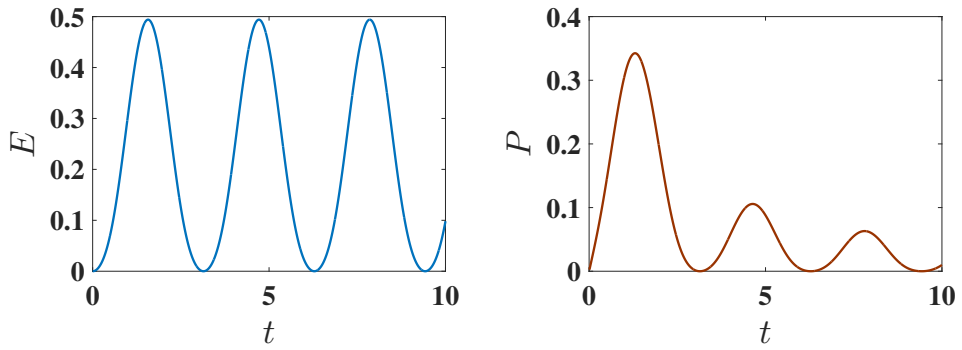


Figure 6. Behavior of (**a**) the stored energy $E(t)$ and (**b**) the average charging power $P(t)$ of the QB as a function of charging time t for $\Delta = -1.5$, corresponding to the ferromagnetic ground state. The charging is performed using the harmonic charging field described by $U(t) = \mathcal{T}\exp(-i\int_0^t H_C(t')dt')$. Other parameters used are $J = 1$, $h = 1$, $\omega = 1$ and $B = 1$.

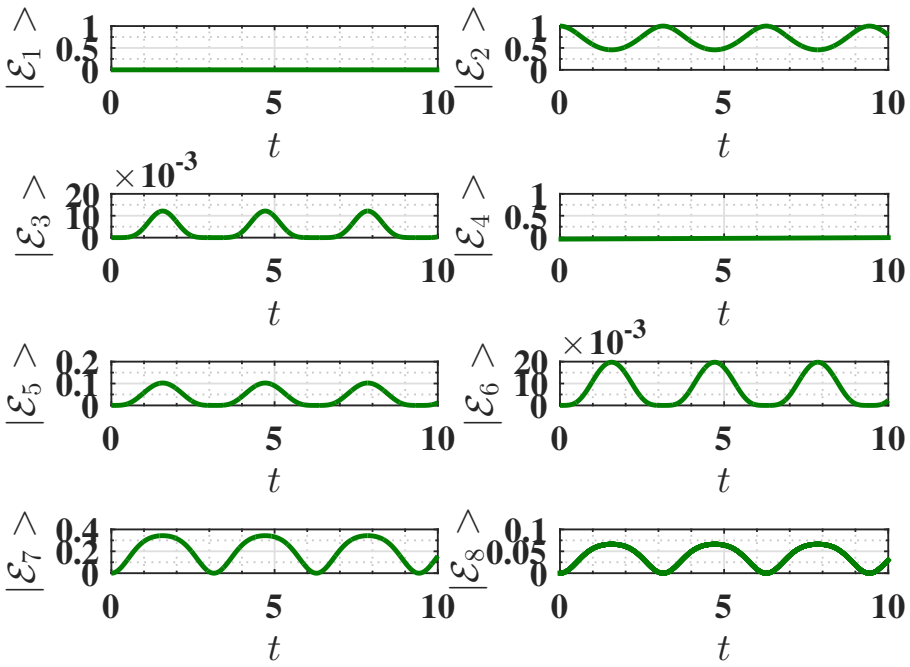


Figure 7. Behavior of the eigenstate populations (see Equation (2)) as a function of charging time t for $\Delta = -1.5$, corresponding to the ferromagnetic ground state. The charging is performed using the harmonic field, with $U(t) = \mathcal{T}\exp(-i\int_0^t H_C(t')dt')$. The parameters are the same as Figure 6. We recall that in our notation, $|\mathcal{E}_2\rangle$ is the ground state, and $|\mathcal{E}_3\rangle$ is the highest excited state (see Equation (2)).

3.2.2. Antiferromagnetic Ground State ($\Delta = -1.6$)

Here, the maximum energy is $E_{\max} = 6.0124$. Interestingly, the antiferromagnetic state shows a more favorable performance under harmonic charging than the ferromagnetic state. As shown in Figure 8a, the energy stored starting from the antiferromagnetic ground state is significantly higher than in the ferromagnetic case. This improved performance is attributed to the more efficient population swap between the ground state ($|\mathcal{E}_7\rangle$) and excited states (specifically the highest energy state $|\mathcal{E}_3\rangle$), as indicated by the eigenstate population dynamics in Figure 9.

The improved performance of harmonic charging in the antiferromagnetic case arises from the fundamental difference in the interaction structure of the spin chain. In a ferromagnetic system, spins naturally align in the same direction, so applying a uniform charging protocol to all spins is relatively efficient. However, in an antiferromagnetic chain, adjacent spins tend to align oppositely, and because of this, applying the same charging field uniformly to all spins is not the most efficient way to transfer energy. The introduction of an oscillatory (harmonic) charging field provides a new timescale in the system, which enables a resonant enhancement of energy transfer between competing spin configurations. In contrast, for the ferromagnetic case, the system is already aligned, so the introduction of periodic driving does not play a crucial role. This suggests that harmonic charging is particularly beneficial when spin interactions create an energetically unfavorable configuration for uniform charging.

The energy storage dynamics for different values of the driving field amplitude B reveal a fundamental difference between the ferromagnetic and antiferromagnetic systems. In the ferromagnetic case, energy absorption remains low for small $B \ll \omega$, as the driving field weakly perturbs the system. In contrast, the antiferromagnetic system exhibits efficient energy absorption even at small B, likely due to enhanced spin correlations that facilitate energy transfer. As B increases, both systems show an increase in energy storage, but the

antiferromagnetic case consistently outperforms the ferromagnetic one. These findings highlight the role of intrinsic spin interactions in determining the efficiency of quantum battery charging under harmonic driving.

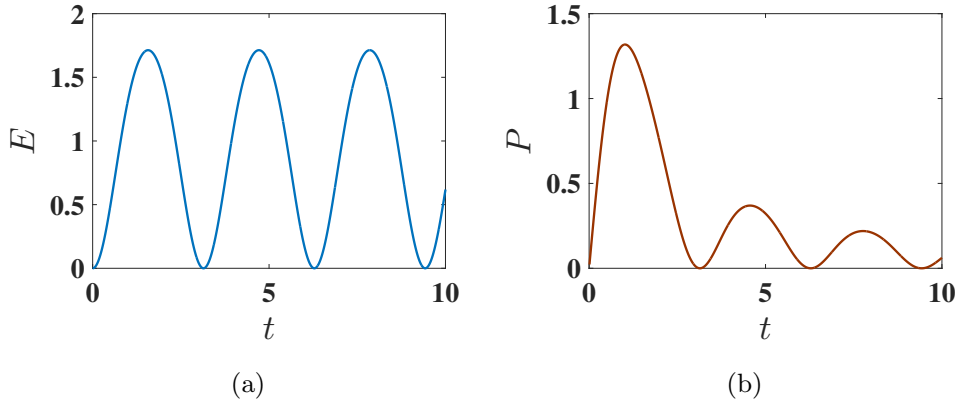


Figure 8. Behavior of (**a**) the stored energy $E(t)$ and (**b**) the average charging power $P(t)$ as a function of charging time t for $\Delta = -1.6$, corresponding to the antiferromagnetic ground state. The charging is performed using the harmonic field, with $U(t) = \mathcal{T}\exp(-i\int_0^t H_C(t')dt')$. Other parameters are the same as Figure 6.

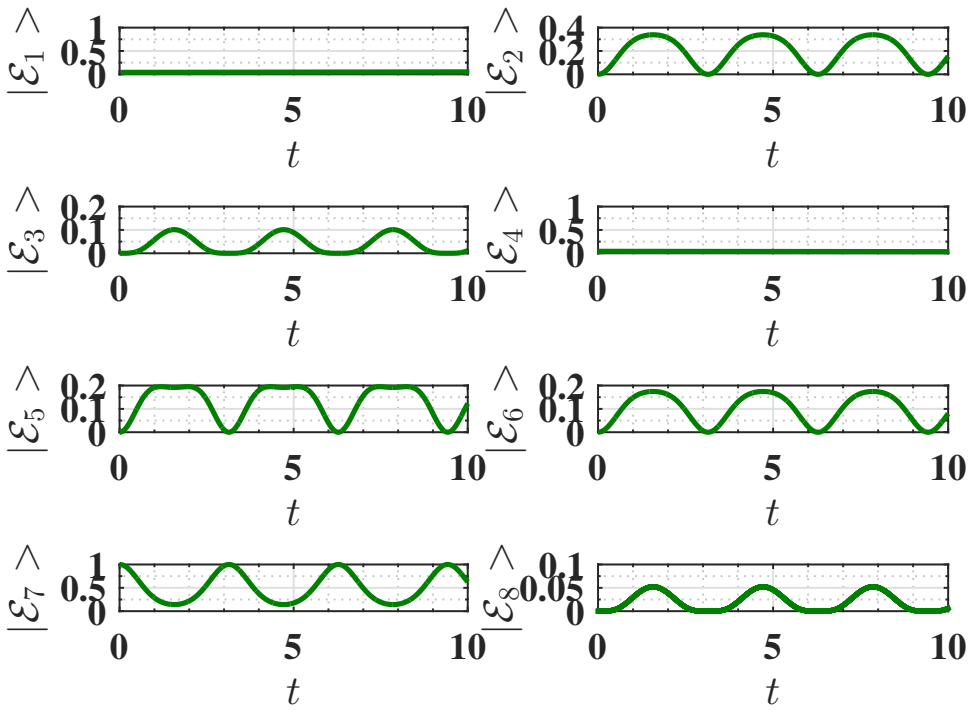


Figure 9. Behavior of the eigenstate populations (see Equation (2)) as a function of charging time t for $\Delta = -1.6$, corresponding to the antiferromagnetic ground state. The charging is performed using the harmonic field, $U(t) = \mathcal{T}\exp(-i\int_0^t H_C(t')dt')$. Other parameters are the same as Figure 6. We recall that in our notation $|\mathcal{E}_7\rangle$ is the ground state, and $|\mathcal{E}_3\rangle$ is the highest excited state (see Equation (2)).

To further characterize the charging process, we investigate the role of quantum coherence as a potential figure of merit for energy storage. Specifically, we analyze the time evolution of the l_1-norm coherence:

$$C(\rho) = \sum_{i \neq j} |\rho_{ij}|$$

where ρ_{ij} are the off-diagonal elements of the density matrix. This measure quantifies the total amount of quantum superposition in the system. We compare the behavior of stored energy and coherence under harmonic driving for ferromagnetic ($\Delta = -1.5$) and antiferromagnetic ($\Delta = -1.6$) cases in Figure 10, which presents the time evolution of stored energy $E(t)$ and coherence $C(\rho)$. In the ferromagnetic case, coherence builds up transiently but is rapidly lost, leading to poor energy storage. By contrast, in the antiferromagnetic case, coherence is sustained throughout the charging process, facilitating stronger energy storage. These results suggest that coherence plays a crucial role in energy transfer, with persistent coherence corresponding to more efficient quantum charging. The findings highlight the importance of long-lived coherence rather than transient effects, reinforcing the role of quantum correlations in energy storage.

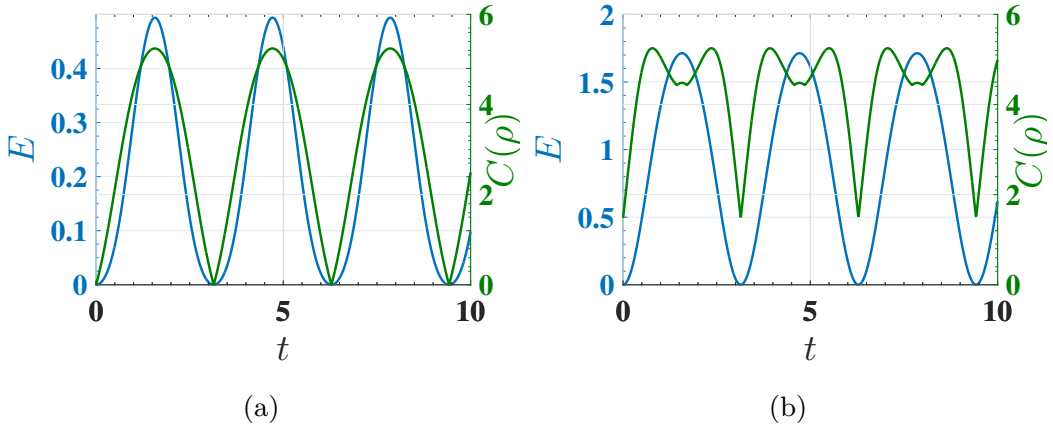


Figure 10. The behavior of the stored energy $E(t)$ (left y-axis) and l_1-norm coherence $C(\rho)$ (right y-axis) for (**a**) the ferromagnetic case ($\Delta = -1.5$) and (**b**) the antiferromagnetic case ($\Delta = -1.6$) as a function of charging time t. These plots illustrate how coherence affects energy storage dynamics, where charging is performed using the harmonic field described by $U(t) = \mathcal{T} \exp(-i \int_0^t H_C(t')dt')$. Sustained coherence in the antiferromagnetic case correlates with higher energy storage, whereas transient coherence in the ferromagnetic case limits energy transfer. Other parameters are the same as in Figure 6.

3.2.3. Maximum Average Power

Comparing Figures 6b and 8b, we observe that under harmonic charging, the maximum average power $P_{\max}$ is significantly higher in the antiferromagnetic case compared to the ferromagnetic one. Interestingly, also for this protocol, $P_{\max}$ is reached faster starting from the antiferromagnetic state than from the ferromagnetic state.

3.3. Joint Evolution Considering QB and Charging Hamiltonians

We present here the results of charging the QB through the joint evolution of the battery Hamiltonian H_B and the charging Hamiltonian H_C.

3.3.1. Static Charging

We consider here the case where the charging process occurs in the presence of both the QB Hamiltonian H_B and the charging Hamiltonian H_C, i.e., the unitary operator leading to the evolution of the initial state of the QB is given by $U(t) = \exp(-i(H_B + H_C)t)$ using static charging method (see Equation (4)). The time evolution of the stored energy $E(t)$ and average power $P(t)$ for both the ferromagnetic and antiferromagnetic initial states under joint evolution is shown in Figure 11. In this scenario, the QB does not achieve the maximum available energy. This can be attributed to the poorer population swap between the ground and excited states. Nonetheless, in the case of the antiferromagnetic initial state, the maximum power $P_{\max}$ is still reached faster than in the ferromagnetic state.

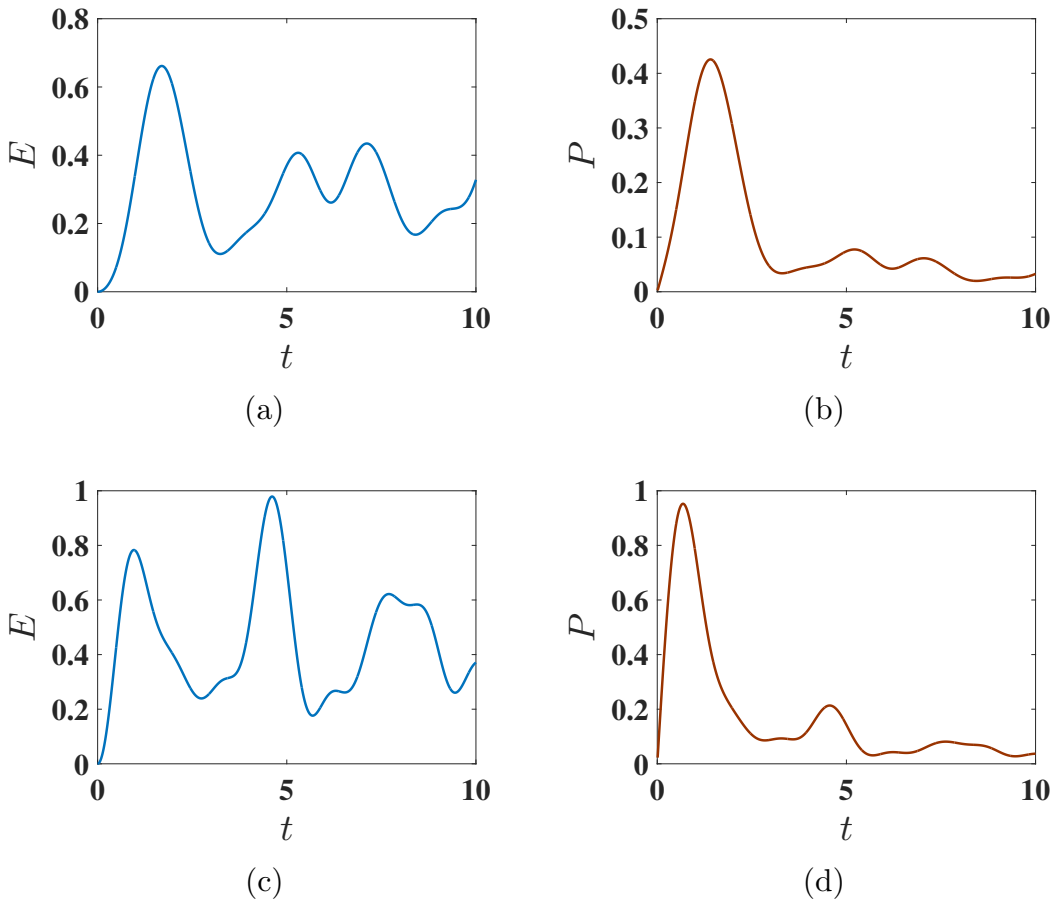


Figure 11. Behavior of the stored energy $E(t)$ and average charging power $P(t)$ as functions of charging time t under the static charging protocol. Panels (**a**,**b**) correspond to the ferromagnetic initial state with $\Delta = -1.5$, while panels (**c**,**d**) correspond to the antiferromagnetic initial state with $\Delta = -1.6$. The charging is performed using the static field $U(t) = \exp(-i(H_B + H_C)t)$. Other parameters are set to $J = 1$, $h = 1$, and $A = 1$.

3.3.2. Harmonic Charging

Here, the initial state of the QB evolves in time according to both H_B and $H_C(t)$, with time evolution governed by the unitary operator $U(t) = \mathcal{T} \exp(-i \int_0^t [H_B + H_C(t')]dt')$, where $\mathcal{T}$ indicates the time ordering. In Figure 12, we display the variation of the stored energy $E(t)$ and average power $P(t)$ for the harmonic charging method (Equation (5)). Similarly to the static case, the QB does not reach maximum charging. However, the charging speed improves, especially in the antiferromagnetic state, where $P_{\max}$ is reached faster. Overall, joint evolution allows faster charging compared to the isolated charging field alone, but at the cost of reduced energy output. Interestingly, the antiferromagnetic case consistently shows faster charging compared to the ferromagnetic one.

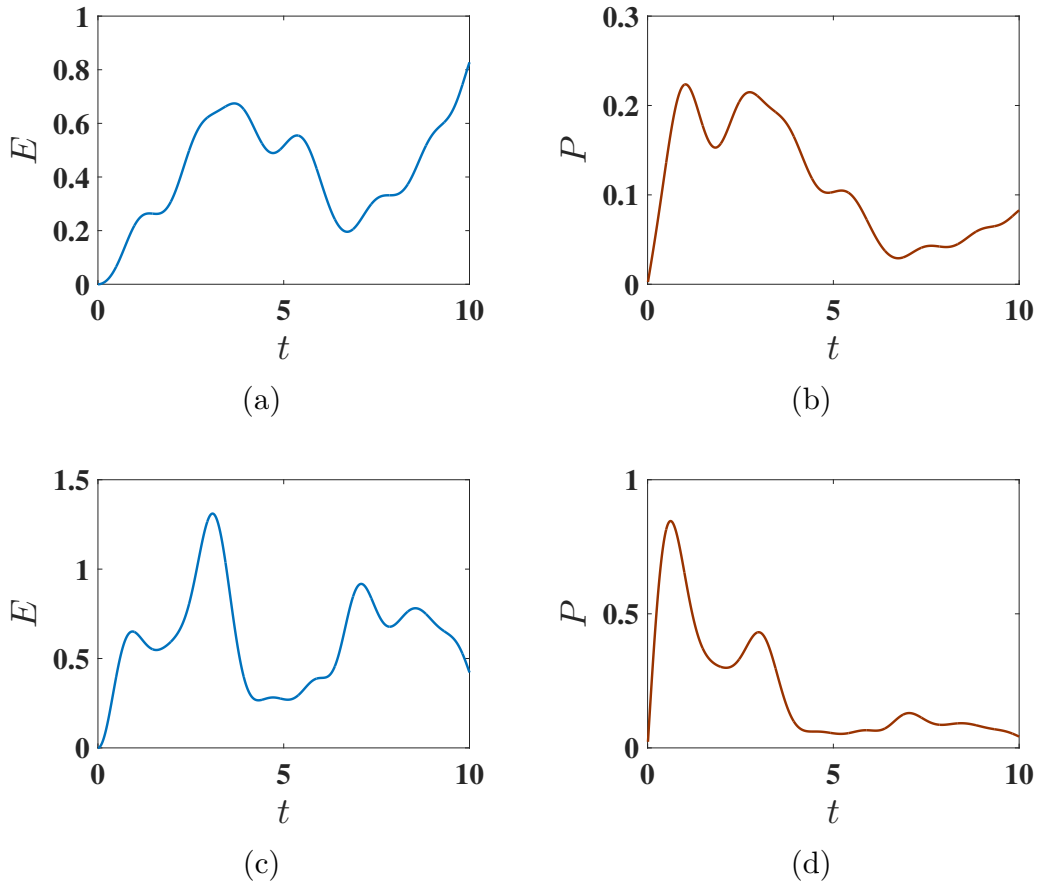


Figure 12. Behavior of the stored energy $E(t)$ and average charging power $P(t)$ as functions of charging time t under the harmonic charging method. Panels (**a**,**b**) correspond to the ferromagnetic initial state with $\Delta = -1.5$, while panels (**c**,**d**) correspond to the antiferromagnetic initial state with $\Delta = -1.6$. The charging is performed using the harmonic field described by $U(t) = \mathcal{T}\exp(-i\int_0^t [H_B + H_C(t')]dt')$. Other parameters are set as $J = 1$, $h = 1$, $\omega = 1$, and $B = 1$.

4. Conclusions

In this work, we investigated the charging performance of a quantum battery composed of three qubits, modeled as a spin system with XXZ coupling. By considering both static and harmonic charging mechanisms, we observed distinct behaviors depending on the nature of the initial condition, namely ferromagnetic or antiferromagnetic, achieved by moving the anisotropy parameter Δ above and below a numerically determined crossover value Δ_C, respectively.

Starting from a ferromagnetic ground state, characterized by $\Delta > \Delta_C$, the system exhibits well-aligned spins, allowing efficient population transfer between the ground state $|\mathcal{E}_2\rangle$ and the excited state $|\mathcal{E}_3\rangle$. Under static charging, the system reaches its maximum achievable energy, as reflected in the stored energy and average charging power. In contrast, harmonic charging under these conditions fails to reach the same energy levels due to incomplete population transfer caused by the oscillatory nature of the driving field.

In the antiferromagnetic case, where $\Delta < \Delta_C$, static charging struggles to achieve high energy levels, whereas harmonic charging performs significantly better. The oscillatory field facilitates population transfer, resulting in higher stored energy and faster charging times. These findings suggest that the choice of charging mechanism should be tailored to the initial state of the quantum battery to optimize its performance.

Our analysis also reveals that quantum coherence serves as a meaningful figure of merit for characterizing quantum battery charging for harmonic charging. The ferromag-

netic case ($\Delta = -1.5$) exhibits transient coherence that quickly disappears, leading to poor energy storage. In contrast, the antiferromagnetic case ($\Delta = -1.6$) maintains more stable coherence, which correlates with higher energy absorption and better charging performance. These findings suggest that the sustained presence of coherence, rather than its instantaneous peak, plays a crucial role in enhancing quantum battery efficiency.

We also analyzed the more realistic joint evolution of the QB under the combined influence of the QB Hamiltonian and the charging Hamiltonian for both static and harmonic fields. In this case, we observed that while the quantum battery does not reach its maximum energy capacity, the charging process is accelerated in the antiferromagnetic case, highlighting the role of anisotropy in optimizing charging efficiency. This effect is likely due to the competition between spin interactions, which enhances the system's ability to absorb energy over shorter time periods, albeit at the cost of reduced overall energy output.

We have focused on a small system size $N = 3$, to explore the fundamental role of initial conditions and charging protocols. However, the scaling of maximum charging energy with system size is an important question in spin-based quantum batteries, and a detailed numerical study of this effect in our system represents an important future development of this work. Moreover, we have highlighted the importance of the initial conditions in determining the optimal charging strategy for QB. Future research could explore more complex spin systems or alternative coupling mechanisms, which may reveal additional quantum advantages in energy storage.

Author Contributions: Conceptualization, S.C., D.F. and N.T.Z.; formal analysis, S.C.; writing—original draft preparation, S.C.; writing—review and editing, D.F. and N.T.Z.; supervision, D.F. and N.T.Z. All authors have read and agreed to the published version of the manuscript.

Funding: S.C. and N.T.Z. acknowledge the funding through the NextGenerationEu Curiosity-Driven Project "Understanding even-odd criticality". N.T.Z. acknowledges the funding through the "Non-reciprocal supercurrent and topological transitions in hybrid Nb- InSb nanoflags" project (Prot. 2022PH852L) in the framework of PRIN 2022 initiative of the Italian Ministry of University (MUR) for the National Research Program (PNR). This project has been funded within the programme "PNRR Missione 4-Componente 2-Investimento 1.1 Fondo per il Programma Nazionale di Ricerca e Progetti di Rilevante Interesse Nazionale (PRIN)". S.C. and D.F. acknowledge the contribution of the European Union-NextGenerationEU through the "Quantum Busses for Coherent Energy Transfer" (QUBERT) project, in the framework of the Curiosity-Driven 2021 initiative of the University of Genova and through the "Solid State Quantum Batteries: Characterization and Optimization" (SoS-QuBa) project (Prot. 2022XK5CPX), in the framework of the PRIN 2022 initiative of the Italian Ministry of University (MUR) for the National Research Program (PNR). This project has been funded within the programme "PNRR Missione 4-Componente 2-Investimento 1.1 Fondo per il Programma Nazionale di Ricerca e Progetti di Rilevante Interesse Nazionale (PRIN)".

Institutional Review Board Statement: Not applicable.

Informed Consent Statement: Not applicable.

Data Availability Statement: The data presented in this study are available on request from the corresponding author.

Conflicts of Interest: The authors declare no conflicts of interest.

Abbreviations

The following abbreviations are used in this manuscript:

QB	Quantum battery
QPT	Quantum phase transition

References

1. Campaioli, F.; Pollock, F.A.; Vinjanampathy, S. Quantum batteries. In *Thermodynamics in the Quantum Regime*; Binder, F., Correa, L.A., Gogolin, C., Anders, J., Adesso, G., Eds.; Springer: Berlin, Germany, 2018; pp. 207–225. [CrossRef]
2. Bhattacharjee, S.; Dutta, A. Quantum thermal machines and batteries. *Eur. Phys. J. B* **2021**, *94*, 1–42. [CrossRef]
3. Quach, J.Q.; Cerullo, G.; Virgili, T. Quantum batteries: The future of energy storage? *Joule* **2023**, *7*, 2195–2200. [CrossRef]
4. Campaioli, F.; Gherardini, S.; Quach, J.Q.; Polini, M.; Andolina, G.M. Colloquium: Quantum batteries. *Rev. Mod. Phys.* **2024**, *96*, 031001. [CrossRef]
5. Jaeger, L. *The Second Quantum Revolution*; Springer Nature: Cham, Switzerland, 2018. [CrossRef]
6. Benenti, G.; Casati, G.; Rossini, D.; Strini, G. *Principles of Quantum Computation and Information : A Comprehensive Textbook*; World Scientific: Singapore, 2018. [CrossRef]
7. Esposito, M.; Harbola, U.; Mukamel, S. Nonequilibrium fluctuations, fluctuation theorems, and counting statistics in quantum systems. *Rev. Mod. Phys.* **2009**, *81*, 1665–1702. [CrossRef]
8. Vinjanampathy, S.; Anders, J. Quantum thermodynamics. *Contemp. Phys.* **2016**, *57*, 545–579. [CrossRef]
9. Campisi, M.; Fazio, R. Dissipation, correlation and lags in heat engines. *J. Phys. A Math. Theor.* **2016**, *49*, 345002. [CrossRef]
10. Benenti, G.; Casati, G.; Saito, K.; Whitney, R.S. Fundamental aspects of steady-state conversion of heat to work at the nanoscale. *Phys. Rep.* **2017**, *694*, 1–124. [CrossRef]
11. Potts, P.P. Quantum Thermodynamics. *arXiv* **2024**. arXiv:2406.19206. [CrossRef]
12. de Paula, V.G.; Santana, W.S.; Cruz, C.; Reis, M. Quantum Thermodynamics in Spin Systems: A Review of Cycles and Applications. *arXiv* **2024**. arXiv:2411.12470. [CrossRef]
13. Alicki, R.; Fannes, M. Entanglement boost for extractable work from ensembles of quantum batteries. *Phys. Rev. E* **2013**, *87*, 042123. [CrossRef]
14. Binder, F.C.; Vinjanampathy, S.; Modi, K.; Goold, J. Quantacell: Powerful charging of quantum batteries. *New J. Phys.* **2015**, *17*, 075015. [CrossRef]
15. Campaioli, F.; Pollock, F.A.; Binder, F.C.; Céleri, L.; Goold, J.; Vinjanampathy, S.; Modi, K. Enhancing the Charging Power of Quantum Batteries. *Phys. Rev. Lett.* **2017**, *118*, 150601. [CrossRef] [PubMed]
16. Andolina, G.M.; Farina, D.; Mari, A.; Pellegrini, V.; Giovannetti, V.; Polini, M. Charger-mediated energy transfer in exactly solvable models for quantum batteries. *Phys. Rev. B* **2018**, *98*, 205423. [CrossRef]
17. Julià-Farré, S.; Salamon, T.; Riera, A.; Bera, M.N.; Lewenstein, M. Bounds on the capacity and power of quantum batteries. *Phys. Rev. Res.* **2020**, *2*, 023113. [CrossRef]
18. Rosa, D.; Rossini, D.; Andolina, G.M.; Polini, M.; Carrega, M. Ultra-stable charging of fast-scrambling SYK quantum batteries. *J. High Energy Phys.* **2020**, *2020*, 67. [CrossRef]
19. Rossini, D.; Andolina, G.M.; Rosa, D.; Carrega, M.; Polini, M. Quantum Advantage in the Charging Process of Sachdev-Ye-Kitaev Batteries. *Phys. Rev. Lett.* **2020**, *125*, 236402. [CrossRef] [PubMed]
20. Gyhm, J.-Y.; Šafránek, D.; Rosa, D. Quantum Charging Advantage Cannot Be Extensive Without Global Operations. *Phys. Rev. Lett.* **2022**, *128*, 140501. [CrossRef]
21. Crescente, A.; Ferraro, D.; Carrega, M.; Sassetti, M. Enhancing coherent energy transfer between quantum devices via a mediator. *Phys. Rev. Res.* **2022**, *4*, 033216. [CrossRef]
22. Hu, C.-K.; Qiu, J.; Souza, P.J.P.; Yuan, J.; Zhou, Y.; Zhang, L.; Chu, J.; Pan, X.; Hu, L.; Li, J.; et al. Optimal charging of a superconducting quantum batteries. *Quantum Sci. Technol.* **2022**, *7*, 045018. [CrossRef]
23. Mazzoncini, F.; Cavina, V.; Andolina, G.M.; Erdman, P.A.; Giovannetti, V. Optimal control methods for quantum batteries. *Phys. Rev. A* **2023**, *107*, 032218. [CrossRef]
24. Morrone, D.; Rossi, M.A.C.; Genoni, M.G. Daemonic ergotropy in continuously monitored open quantum batteries. *Phys. Rev. Appl.* **2023**, *20*, 044073. [CrossRef]
25. Gemme, G.; Grossi, M.; Vallecorsa, S.; Sassetti, M.; Ferraro, D. Qutrit quantum battery: Comparing different charging protocols. *Phys. Rev. Res.* **2024**, *6*, 023091. [CrossRef]
26. Razzoli, L.; Gemme, G.; Khomchenko, I.; Sassetti, M.; Ouerdane, H.; Ferraro, D.; Benenti, G. Cyclic solid-state quantum battery: thermodynamic characterization and quantum hardware simulation. *Quantum Sci. Technol.* **2025**, *10*, 015064. [CrossRef]
27. Cavaliere, F.; Gemme, G.; Benenti, G.; Ferraro, D.; Sassetti, M. Dynamical Blockade of a reservoir for optimal performances of a quantum battery. *Commun. Phys.* **2025**, *8*, 76. [CrossRef]
28. Ferraro, D.; Campisi, M.; Andolina, G.M.; Pellegrini, V.; Polini, M. High-Power Collective Charging of a Solid-State Quantum Battery. *Phys. Rev. Lett.* **2018**, *120*, 117702. [CrossRef]
29. Andolina, G.M.; Keck, M.; Mari, A.; Giovannetti, V.; Polini, M. Quantum versus classical many-body batteries. *Phys. Rev. B* **2019**, *99*, 205437. [CrossRef]
30. Quach, J.Q.; McGhee, K.E.; Ganzer, L.; Rouse, D.M.; Lovett, B.W.; Gauger, E.M.; Keeling, J.; Cerullo, G.; Lidzey, D.G.; Virgili, T. Superabsorption in an organic microcavity: Toward a quantum battery. *Sci. Adv.* **2022**, *8*, eabk3160. [CrossRef]

31. Dou, F.-Q.; Lu, Y.-Q.; Wang, Y.-J.; Sun, J.-A. Extended Dicke quantum battery with interatomic interactions and driving field. *Phys. Rev. B* **2022**, *105*, 115405. [CrossRef]
32. Erdman, P.A.; Andolina, G.M.; Giovannetti, V.; Noé, F. Reinforcement Learning Optimization of the Charging of a Dicke Quantum Battery. *Phys. Rev. Lett.* **2024**, *133*, 243602. [CrossRef]
33. Gyhm, J.-Y.; Fischer, U.R. Beneficial and detrimental entanglement for quantum battery charging. *AVS Quantum Sci.* **2024**, *6*, 012001. [CrossRef]
34. Ahmadi, B.; Mazurek, P.; Horodecki, P.; Barzanjeh, S. Nonreciprocal Quantum Batteries. *Phys. Rev. Lett.* **2024**, *132*, 210402. [CrossRef]
35. Elyasi, S.N.; Rossi, M.A.C.; Genoni, M.G. Experimental simulation of daemonic work extraction in open quantum batteries on a digital quantum computer. *Quantum Sci. Tech.* **2025**, *10*, 025017. [CrossRef]
36. Hadipour, M.; Haseli, S.; Wang, D.; Haddadi, S. Proposed Scheme for a Cavity-Based Quantum Battery. *Adv. Quantum Technol.* **2024**, *7*, 2400115. .. [CrossRef]
37. Hadipour, M.; Haseli, S.; Dolatkhah, H.; Rashidi, M. Study the charging process of moving quantum batteries inside cavity. *Sci. Rep.* **2023**, *13*, 10672. [CrossRef] [PubMed]
38. Le, T.P.; Levinsen, J.; Modi, K.; Parish, M.M.; Pollock, F.A. Spin-chain model of a many-body quantum battery. *Phys. Rev. A* **2018**, *97*, 022106. [CrossRef]
39. Verma, D.; Indrajith, V.S.; Sankaranarayanan, R. Dynamics of Heisenberg XYZ two-spin quantum battery. *Physica A* **2025**, *659*, 130352. [CrossRef]
40. Yang, H.-Y.; Zhang, K.; Wang, X.-H.; Shi, H.-L. Optimal energy storage and collective charging speedup in the central-spin quantum battery. *Phys. Rev. B* **2025**, *111*, 085410. [CrossRef]
41. Ali, A.; Elghaayda, S.; Al-Kuwari, S.; Hussain, M.I.; Rahim, M.T.; Kuniyil, H.; Seida, C.; El Allati, A.; Mansour, M.; Haddadi, S. Kitaev Quantum Batteries: Super-Extensive Scaling of Ergotropy in 1D Spin-1/2 XY-$\Gamma(\gamma)$ Chain. *arXiv* **2024**, arXiv:2411.14074. [CrossRef]
42. Zhang, X.-L.; Song, X.-K.; Wang, D. Quantum Battery in the Heisenberg Spin Chain Models with Dzyaloshinskii-Moriya Interaction. *Adv. Quantum Technol.* **2024**, *7*, 2400114. [CrossRef]
43. Rahman, S.; Murugesh, S. Effect of DM Interaction in the charging process of a Heisenberg spin chain quantum battery. *Phys. Scr.* **2024**, *100*, 015106. [CrossRef]
44. Ali, A.; Al-Kuwari, S.; Hussain, M.I.; Byrnes, T.; Rahim, M.T.; Quach, J.Q.; Ghominejad, M.; Haddadi, S. Ergotropy and capacity optimization in Heisenberg spin-chain quantum batteries. *Phys. Rev. A* **2024**, *110*, 052404. [CrossRef]
45. Franchini, F. *An Introduction to Integrable Techniques for One-Dimensional Quantum Systems*; Springer: Berlin/Heidelberg, Germany, 2017. [CrossRef]
46. Porta, S.; Cavaliere, F.; Sassetti, M.; Traverso Ziani, N. Topological classification of dynamical quantum phase transitions in the xy chain. *Sci. Rep.* **2020**, *10*, 12766. [CrossRef] [PubMed]
47. Sacco Shaikh, D.; Catalano, A.G.; Cavaliere, F.; Franchini, F.; Sassetti, M.; Traverso, Ziani, N. Phase diagram of the topologically frustrated XY chain. *Eur. Phys. J. Plus* **2024**, *139*, 1–14. [CrossRef]
48. Barra, F.; Hovhannisyan, K.V.; Imparato, A. Quantum batteries at the verge of a phase transition. *New J. Phys.* **2022**, *24*, 015003. [CrossRef]
49. Campisi, M.; Fazio, R. The power of a critical heat engine. *Nat. Commun.* **2016**, *7*, 11895. [CrossRef]
50. Chand, S.; Biswas, A. Critical-point behavior of a measurement-based quantum heat engine. *Phys. Rev. E* **2018**, *98*, 052147. [CrossRef]
51. Caravelli, F.; Yan, B.; García-Pintos, L.P.; Hamma, A. Energy storage and coherence in closed and open quantum batteries. *Quantum* **2021**, *5*, 505. [CrossRef]
52. Grazi, R.; Sacco Shaikh, D.; Sassetti, M.; Traverso Ziani, N.; Ferraro, D. Controlling Energy Storage Crossing Quantum Phase Transitions in an Integrable Spin Quantum Battery. *Phys. Rev. Lett.* **2024**, *133*, 197001. [CrossRef]
53. Grazi, R.; Cavaliere, F.; Traverso Ziani, N.; Ferraro, D. Charging a Dimerized Quantum XY Chain. *Symmetry* **2025**, *17*, 220. [CrossRef]
54. Grazi, R.; Cavaliere, F.; Sassetti, M.; Ferraro, D.; Traverso Ziani, N. Charging Free Fermion Quantum Batteries. *Chaos, Solitons & Fractals* **2025**, *196*, 116383. [CrossRef]
55. Catalano, A.G.; Giampaolo, S.M.; Morsch, O.; Giovannetti, V.; Franchini, F. Frustrating Quantum Batteries. *Phys. Rev. X Quantum* **2024**, *5*, 030319. [CrossRef]
56. Jafari, R.; Langari, A. Three-qubits ground state and thermal entanglement of anisotropic Heisenberg (XXZ) and ising models with Dzyaloshinskii-Moriya interaction. *Int. J. Quantum Inf.* **2011**, *9*, 1057–1079. [CrossRef]
57. Yong, Z.; Gui-Lu, L. Ground-State and Thermal Entanglement in Three-Spin Heisenberg-XXZ Chain with Three-Spin Interaction. *Commun. Theor. Phys.* **2007**, *48*, 249. [CrossRef]

58. Ali, A.; Elghaayda, S.; Al-Kuwari, S.; Hussain, M.I.; Rahim, M.T.; Kuniyil, H.; Byrnes, T.; Quach, J.Q.; Mansour, M.; Haddadi, S. Magnetic Dipolar Quantum Battery with Spin-Orbit Coupling. *arXiv* **2024**, arXiv:2409.05000. [CrossRef]
59. Yan, Y.; Lü, Z.; Zheng, H. Bloch-Siegert shift of the Rabi model. *Phys. Rev. A* **2015**, *91*, 053834. [CrossRef]
60. Yu, Y.; Chen, A. Quantum Battery Based on Hybrid Field Charging. *Entropy* **2022**, *24*, 1821. [CrossRef]
61. Ghosh, S.; Chanda, T.; Sen(De), A. Enhancement in the performance of a quantum battery by ordered and disordered interactions. *Phys. Rev. A* **2020**, *101*, 032115. [CrossRef]
62. Mondal, S.; Bhattacharjee, S. Periodically driven many-body quantum battery. *Phys. Rev. E* **2022**, *105*, 044125. [CrossRef]
63. Huang, X.; Wang, K.; Xiao, L.; Gao, L.; Lin, H.; Xue, P. Demonstration of the charging progress of quantum batteries. *Phys. Rev. A* **2023**, *107*, L030201. [CrossRef]
64. Zhang, Y.-Y.; Yang, T.-R.; Fu, L.; Wang, X. Powerful harmonic charging in a quantum battery. *Phys. Rev. E* **2019**, *99*, 052106. [CrossRef]
65. Wen, J.; Wen, Z.; Peng, P.; Li, G.-Q. Dicke-Ising quantum battery of an ion chain driven by a mechanical oscillator. *arXiv* **2025**, arXiv:2502.08065. [CrossRef]
66. Elghaayda, S.; Ali, A.; Al-Kuwari, S.; Czerwinski, A.; Mansour, M.; Haddadi, S. Performance of a Superconducting Quantum Battery. *Adv. Quantum Technol.* **2025**, 2400651. [CrossRef]

Disclaimer/Publisher's Note: The statements, opinions and data contained in all publications are solely those of the individual author(s) and contributor(s) and not of MDPI and/or the editor(s). MDPI and/or the editor(s) disclaim responsibility for any injury to people or property resulting from any ideas, methods, instructions or products referred to in the content.